This document is confidential and is proprietary to the American Chemical Society and its authors. Do not copy or disclose without written permission. If you have received this item in error, notify the sender and delete all copies.

# Bioavailability Enhancing Cocrystals: screening, in vivo predicative dissolution, and supersaturation maintenance

Journal:	Crystal Growth & Design		
Manuscript ID	cg-2021-00950d.R4		
Manuscript Type:	Article		
Date Submitted by the Author:	18-Jul-2022		
Complete List of Authors:	Chen, Dabing; Boehringer Ingelheim Pharmaceuticals Inc, Material and analytical science Huang, Wenjun; Boehringer Ingelheim Corp USA Sun, Qinfang; Boehringer Ingelheim Corp USA Zhang, Zenghui; Boehringer Ingelheim Corp USA Guo, Yiwang; University of Minnesota Twin Cities, College of Pharmacy Vreeman, Gerrit; University of Minnesota Department of Pharmaceutics, Pharmaceutics Sun, Changquan; University of Minnesota Twin Cities, Pharmaceutics Hawley, Michael; Boehringer Ingelheim Corp USA Yang, Bing-Shiou; Boehringer Ingelheim Pharmaceuticals Inc, He, Xiaorong; Boehringer Ingelheim Corp USA		

SCHOLARONE™ Manuscripts Bioavailability Enhancing Cocrystals: screening, in vivo predictive dissolution, and supersaturation maintenance

Dabing Chen<sup>1,3\*</sup>, Wenjun Huang<sup>1</sup>, Qinfang Zhang<sup>1</sup>, Zenghui Zhang<sup>1</sup>, Yiwang Guo<sup>2</sup>, Gerrit Vreeman<sup>2</sup>, Changquan Calvin Sun<sup>2\*</sup>, Michael Hawley<sup>1</sup>, Bing-Shiou Yang<sup>1</sup>, Xiaorong He<sup>1</sup>

College of Pharmacy, University of Minnesota, Minneapolis, MN 55455, United States

<sup>&</sup>lt;sup>1</sup>Boehringer Ingelheim Pharmaceuticals Inc., 900 Ridgebury Road, Ridgefield, CT 06877, USA

<sup>&</sup>lt;sup>2</sup> Pharmaceutical Materials Science and Engineering Laboratory, Department of Pharmaceutics,

<sup>&</sup>lt;sup>3</sup> Currently Formulation R&D, Arvinas, New Haven, CT 06510, USA

<sup>\*</sup> corresponding authors

# Abstract

Cocrystal engineering for bioavailability enhancement is still a serendipitous process, which requires systematic solution crystallization, in vivo predictive dissolution, and biopharmaceutical simulation. The purpose of this study is to improve bioavailability through cocrystal engineering. with a focus on understanding the mechanism of supersaturation maintenance during dissolution. BI 639667 is a poorly soluble and fast precipitating compound. The ability of its cocrystal with salicylic acid to maintain supersaturation was assessed using a modified two-step dissolution method, and its bioavailability was determined in rats. Biopharmaceutical simulation and dissolution modeling were performed to predict the *in vivo* performance in humans. COSMO-RS and molecular dynamics simulation (MD) were used to study the interactions between API and coformers in a vacuum and aqueous media, respectively. A high melting cocrystal with salicylic acid (SA), crystallized in dichloromethane, showed moderate solubility enhancement with prolonged supersaturation during dissolution, which was able to enhance bioavailability with reduced  $C_{\text{max}}$ , compared to amorphous dispersion. The radial distribution function (RDF) between API and selected coformers was calculated using MD simulation to determine the mean distance between API and coformer molecules in aqueous media. The result suggests that SA could better compete against water for interactions with the API and could penetrate the API molecular clusters to inhibit nucleation. Thus, the RDF by MD simulation may be used to determine the disruptive effect of water on the interaction between API and coformer and improve cocrystal engineering for bioavailability enhancement.

- Keywords: Bioavailability, Cocrystal, Supersaturation, *In vivo* predicative dissolution,
- 24 Biopharmaceutical simulation, Molecular dynamics

3.5

# Introduction

Cocrystals are crystalline single-phase materials composed of two or more different molecular and/or ionic compounds generally in a stoichiometric ratio that are neither solvates nor simple salts [1]. The first cocrystal of quinone and hydroquinone was reported in 1844 [2]. Hydrogen bonding rules for designing organic cocrystals was proposed by Etter et al. in 1990 [3]. The concept of supramolecular synthon or hydrogen-bonded building units was later developed by Desiraju [4]. Cocrystal formation has become a powerful tool for enhancing key pharmaceutical properties [5], including stability [6], dissolution [7, 8]; bioavailability [9], and manufacturability [10] in the industry. Other applications, such as taste masking [11] and toxicity reduction [12], have also been reported. Hence, cocrystal formation has become an attractive crystal engineering approach for improving the performance of poorly soluble compounds, especially when a suitable salt cannot be attained or when the compounds are not ionizable. FDA has provided guideline on cocrystals for the pharmaceutical industry with the most recent update in 2018 [13]. The first tablet product of a pharmaceutical ionic cocrystal, Entresto, was launched in 2015 by Novartis.

Amorphous dispersion and co-crystallization are two common techniques used to enhance the bioavailability of poorly soluble compounds. Compared to amorphous dispersions, cocrystal materials usually show advantages in term of processability, tabletability and flowability [14]. Manufacturing cocrystals at a large scale is facilitated by a clear understanding of the tertiary phase diagram of API, cocrystal former (or conformer), and solvent [15]. To enhance solubility by a cocrystal, a coformer having a high aqueous solubility is usually selected, and the cocrystal solubility generally increases with that of the coformer [16]. The solubility enhancement can be 10-20 fold higher [17]. Similar to salts and amorphous materials, cocrystals may enhance bioavailability of a poorly soluble drug through via the spring and parachute mechanism [18]. However, phase transformation back to the parent drug during storage or dissolution in GI fluid may negate the solubility advantage afforded by the soluble cocrystals.

Despite the progress in the past decade, cocrystal development for bioavailability enhancement is still an empirical and serendipitous process. An outstanding problem is that the solubility enhancement is not always predictive of the bioavailability enhancement since the solubility of cocrystal does not strongly correlate with the *in vivo* performance [19]. For example, AMG 517 sorbic acid cocrystal showed good aqueous solubility but did not show enhanced *in vivo* performance compared with the free form [20]. A recent study reported that, among the 64 out of 1,000 reported cocrystals having *in vivo* data, most of them only showed less than 4 fold bioavailability enhancement, despite drastic solubility increases [21]. Furthermore, there are 20% of the 64 cocrystals that exhibited increase in bioavailability with reduced solubility or the reverse.

Clearly, the bioavailability of cocrystals is related to more than just their solubility. Therefore, in vitro assessment needs to be improved to better predict the *in vivo* performance of cocrystals. Blindly pursuing a high solubility cocrystal without consideration of supersaturation maintenance can sometimes be counterproductive. One factor to consider is that cocrystals may undergo phase transformation into a less soluble solid form of the parent drug [22]. In this regard, the cocrystal's ability to maintain supersaturation may play an important role in enhancing in vivo performance. In the spring-and-parachute analogy [18], precipitation inhibition by using appropriate inhibitors in tablet formulation could extend the parachute portion to enhance the bioavailability of cocrystals [23, 24]. However, cocrystals that have an intrinsic ability to maintain supersaturation would be more desirable because it reduces formulation complexity and shortens the drug development time. For example, the cilostazol cocrystal with high solubility suffered from fast precipitation and, therefore, poor bioavailability, while the cocrystal with a lower solubility was able to maintain longer supersaturation and higher bioavailability [25]. Search for such cocrystals requires a clear understanding of the mechanism of supersaturation maintenance by cocrystals. To that end, it is useful to ask the following questions: 1) Do coformers maintain supersaturation with a similar mechanism that polymeric precipitation inhibitors do? 2) Which in silico parameters could be used to predict supersaturation maintenance? 3) what is the most effective approach for the development of bioavailability enhancing cocrystal at current time?

The purpose of this work is to understand the mechanism of maintaining supersaturation by cocrystals in aqueous media, and to improve cocrystal engineering methodologies for bioavailability enhancement. The current cocrystal engineering methodologies are mainly based on synthon/hydrogen bonding motifs between API and coformer [4], and enthalpy of cocrystallization [26]. However, in an aqueous solution, this enthalpy change and hydrogen bonding can be greatly affected by water. It is, therefore, important to study the interactions between API and coformer in presence of water to better understand the ability of cocrystal to maintain supersaturation.

The model compound in this study, BI 639667 (Figure 1), is a CCR1 antagonist for rheumatoid arthritis. It showed poor aqueous solubility and fast precipitation kinetics. The supersaturation maintenance capability was tested using a modified two-step dissolution approach. The in vivo performance was determined in rats. Biopharmaceutical simulation coupled with dissolution modeling was employed to predict the *in vivo* performance in humans. The enthalpy of binary interactions between API and different coformers was calculated using COSMO-RS. The interactions between API and coformer in presence of water was studied using molecular dynamic simulations.

# BI 639667

### Coformers considered:

Gentisic acid Salicylic acid

Figure 1 Molecular structures of BI 639667 and selected coformers

# Materials and Methods:

## Materials

1
2
3
_
4 5 6 7
5
6
7
8
9
8 9 10
11
12
14
15
15 16 17
17
18
19
20
21
21 22
23
23
24
25 26 27
26
27
28
29
30
31
21
32
33
34
35 36
36
37
38
39
40
41
42
43
44
45
46
47
48
49
50
51
52
53
54
55

FaSSIF powder was purchased from biorelevent.com. BI 639667 free form was synthesized by
the chemical development department at Boehringer Ingelheim Pharmaceuticals (batch number
B124001105, purity was 99.93% by HPLC). The amorphous dispersion with HPMC-AS was
manufactured using a spray drier (Buchi B290). Methanol was used as the solvent, the inlet and
outlet temperature were set at 100 and 70°C, respectively.

# **Conductor-like Screening Model for Realistic Solvents (COSMO-RS)**

- The interaction energy values between API and coformers were calculated using COSMOtherm software (Version C21, COSMOlogic GmbH, Leverkusen, Germany)) as described before [26].
- The surface charge density was generated using the Turbomole package.

# **Cocrystal screening**

- A methanol solution containing 50 mg of BI 639667 and an equal mole of coformer was dried by nitrogen purge at room temperature. The dried solid was reconstituted with 1 mL of selected
- solvent and equilibrated at room temperature overnight. The remaining solid was harvested by
- filtration and further analyzed.

### SA Cocrystal scale-up

- 1 gram of BI 639667 and 306 mg of salicylic acid were dispersed in 15 mL dichloromethane and
- heated to 50°C for 20 min. The clear solution was filtered through a 0.4 µm PVDF membrane.
- About 1-2 mg of fine SA cocrystal seeds were transferred to the filtrate, which was stirred at RT
- overnight. The cocrystal was harvested by vacuum filtration, followed by drying at 60 °C
- overnight in a vacuum oven. The yield was about 82%.

# **DSC**

- A DSC Q1000 (TA Instruments) was used for differential scanning calorimetry measurements.
- Samples (2-5 milligrams) were placed in crimped aluminum pans with pinhole and heated from
- 20 to 220 °C at 10 °C per minute under nitrogen purge (50 mL/min).

### **Solubility**

Solubility was determined by equilibrating an excess amount of solid in solutions. Samples were shaken at ambient temperature for 2 days. At the end of equilibration, samples were filtered using a 13-mm 0.2-µm PVDF filter and diluted by 11 folds using an ACN/water mixture (1:1, v/v) prior to HPLC analysis.

### **HPLC**

An isocratic HPLC method was used for all measurements. Separation was achieved on a Waters XBridge Shield C18 column (3.0 x 100 mm, 3.5  $\mu$ m) using an Agilent 1100 chromatographic system. A mixture of acetonitrile and 0.1% trifluoracetic acid (30/70, v/v) was used as eluent, with a flow rate of 1 mL/min. The injection volume was either 5 or 10  $\mu$ L. The column was maintained at 35 °C, and the sample compartment was maintained at ambient temperature. The UV detection wavelength was 238 nm. The retention time of BI 639667 was approximately 2.1 minutes.

### **XRPD**

X-Ray powder diffraction studies were conducted using a Bruker D8 Advance with Gobel mirror in parallel beam geometry. Scans were conducted from 3-35° 2-theta at 0.05° step size and 0.6 seconds step time. The diffractometer employed radiation from a Cu anode (1.54 Å) at 40 kV 40 mA. A 1 mm divergence slit was used with the incident beam along with 0.12 mm soller slits in the diffracted beam path. A sodium iodide scintillation detector was used.

### **Single Crystal X-ray Diffraction**

A saturated salicylic acid acetonitrile solution was firstly prepared. This solution was then saturated by BI 639667. Approximately 5 mg BI 639667 powder was added to 3 mL of the above solution, which was heated to obtain a clear solution. The solution was covered with parafilm with small holes introduced and then left for slow evaporation at room temperature. Single crystals were obtained in about 48 hrs. Single crystal X-ray diffraction was performed on a Bruker-AXS Smart diffractometer (Bruker AXS Inc., Madison, Wisconsin), equipped with a Bruker APEX-II CCD detector. The data collection was performed at 100 K with a  $MoK_{\alpha}$  radiation source (graphite monochromator). Data integration was performed with the SAINT program, and the SADABS program was used for scaling and absorption correction, and XPREP

was used for space-group determination and data merging. The crystal structure was solved using SHELXT and refined using the ShelXle program [27]. All hydrogens were placed in ideal positions and refined as riding atoms with relative isotropic displacement parameters. All non-hydrogen atoms were refined with anisotropic displacement parameters. The salicylic acid molecule was modeled as disordered over two positions related by an inversion center. Rietveld refinement was performed using TOPAS (Version 5, Bruker AXS).

# **UV Fiber optic spectroscopy**

The drug concentrations during dissolution and spiking experiments were monitored using a UV fiber optic probe (pION, MA, US). This system utilizes a dip-type UV probe. Six UV fiber optic probes were connected to six miniaturized Photo Diode Array via a fiber optic light guide. A pair of deuterium lamps were used as illumination sources. The data was analyzed using the software package  $\mu$ -diss. The probes were equipped with removable tips, and the path length was 2 mm. As shown in Figure 1, the absorption peak at 258 nm was used for quantification to minimize the interference from salicylic acid, which had an absorbency peak at 240 nm. A baseline correction at 290 nm was applied for concentration measurement.

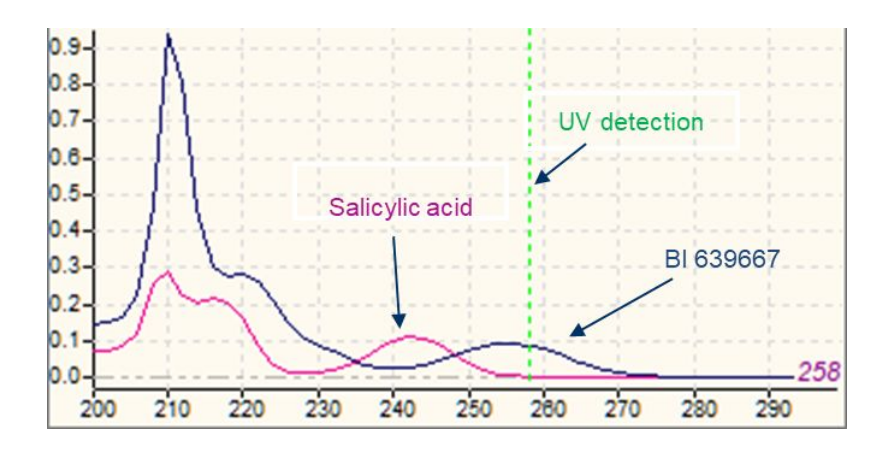


Figure 2 UV spectra of BI 639667 and salicylic acid in FaSSIF at 37 °C

# Precipitation inhibitor screening by solvent shifting method

about 0.1 mL of 30 mg/mL API stock solution in DMSO were pipetted into 15 mL of FaSSIF solutions at 37 °C containing pre-dissolved coformer in FaSSIF,. The API concentration was monitored using an *in situ* fiber optic UV probe.

### Molecular dynamics simulation

The molecular dynamics (MD) simulations were conducted using GROMACS (Ver. 4.6.3). The general Amber force field (GAFF) was used. Force field files were generated using Acpype. 30 molecules of both BI 639667 and each coformer were evenly distributed across a 10x10x10 nm simulation box using Packmol software. The simulation box was then filled with water. The energy minimization was performed in the NPT ensemble using a Nosé-Hoover thermostat and a Parrinello-Rahmam barostat. After the initial energy minimization, the solute and solvent molecules were allowed to move freely. After equilibration for 10 nS, the energy of the system stabilized and reached equilibrium. Production simulation was performed for a maximum of 5,000 steps with the steepest descent algorithm. The convergence criterion of the energy minimization was satisfied when the potential energy reached a plateau, and the maximum force was less than 100 kJ mol<sup>-1</sup>nm<sup>-1</sup>. The *van der* Waals and electrostatic interactions were applied with cutoff distances of 1.0 nm using the Verlet cutoff scheme. The short-range neighbor list was set to 1.0 nm.

### **Modified Two-Step Dissolution**

Dissolution testing was carried out in a USP II apparatus (Vankel VK7000) at 37 °C maintained using an Agilent 750 circulator. Suspension samples were quickly discharged into dissolution media using a pipette. The dissolution media was stirred at 60 rpm using a standard stainless-steel paddle. PEAK 900 mL glass vessels with convex bottoms were used to avoid coning during dissolution. The first dissolution step was conducted in 300 mL of pH 2 HCl solution for 30 minutes, mimicking the stomach condition. The second step involved neutralization with a 5% (w/v) Na<sub>2</sub>HPO<sub>4</sub> solution and held for 2 hours, mimicking the intestine condition. FaSSIF powder was also added to the dissolution media at the second step to mimic human intestinal bile salt levels.

### **Dissolution Modeling and Biopharmaceutical simulation**

To similar dissolution, the formulation is first allowed to disintegrates at a certain rate,  $K_{\rm d}$ . Once disintegrated, the particles will dissolve at the rate determined by particle size, solubility, and hydrodynamics. The dissolved drug was allowed to precipitate as small particles (1  $\mu$ m particle size) when the concentration was greater than the solubility, and the precipitation process was set to follow first-order kinetics. Precipitates would dissolve when the concentration was below their solubility. Second, the dissolved drug was absorbed into the systemic circulation with the absorption rate set as a function of time. Finally, the clearance of the drug in the systemic circulation is assumed to follow first-order kinetics.

The general derivation of Noyes-Whitney expression, developed by Kevin Johnson [1], was used for dissolution simulation. The particles were assumed to be spherical. The particles were binned into 5 bins, i.e., i = 1-5. Within each bin, the particle size was assumed to be uniform to simplify the calculation. The dissolution rate of the crystalline drug was proportional to its solubility, surface area, and diffusion coefficient. It is also dependent on the hydrodynamic conditions.

$$\frac{dXsi}{dt} = \begin{cases} 0, & C_s(t) < \frac{X_d}{V} \\ \frac{-3DX_0^{\frac{1}{3}}X_{si}^{\frac{2}{3}}}{\rho r_0 h} \left(C_s(t) - \frac{X_d}{V}\right) * w, & C_s(t) \ge \frac{X_d}{V} + K_d(t) * \text{Dose} \end{cases}$$
(1)

$$\frac{dX_{p}}{dt} = \begin{cases}
V * \left(\frac{X_{d}}{V} - C_{s}(t)\right) * K_{p}, & C_{s}(t) < \frac{X_{d}}{V} \\
\frac{\frac{1}{3}}{-3DX_{p_{0}}^{3}X_{p}^{3}} \left(C_{s}(t) - \frac{X_{d}}{V}\right) * w, & C_{s}(t) \ge \frac{X_{d}}{V}
\end{cases}$$
(2)

$$\frac{dX_d}{dt} = \sum \sum \frac{3DX_0^{\frac{1}{3}}X_{si}^{\frac{2}{3}}}{\rho r_0 h} \left( C_s(t) - \frac{X_d}{V} \right) * w - \frac{dX_p}{dt} - K_a(t) X_d$$
(3)

$$\frac{dX_a}{dt} = X_d K_a(t) \tag{4}$$

$$\frac{dY}{dt} = \frac{dX_a}{dt} - K_e Y \tag{5}$$

$$\frac{dZ}{dt} = \frac{dY}{dt} / V_d \tag{6}$$

Where  $X_s$  is the mass of API in solids,  $X_0$  is the initial mass of API,  $X_d$  is the mass of dissolved API,  $X_a$  is the mass of absorbed API,  $X_p$  is the mass of precipitated API,  $X_{p0}$  is the maximum mass of precipitated API, Y is the mass of API in central compartment, Z is the concentration of API in central compartment,  $C_s$  (t) is the solubility as the function of time, V is the volume of dissolution media,  $V_d$  is the apparent volume of distribution assuming one compartmental PK model,  $\rho$  is the density of API solids,  $r_0$  is the particle radius of API, h is the thickness of diffusion layer during dissolution, w is the wettability coefficient (0-1),  $K_a$  is the rate of absorption as a function of time,  $K_e$  is the rate of clearance assuming one compartmental PK model,  $K_d$  is the rate of tablet disintegration as a function of time, and  $K_p$  is the precipitation rate constant assuming first order kinetics. The simulation model is graphically shown in Figure 3.

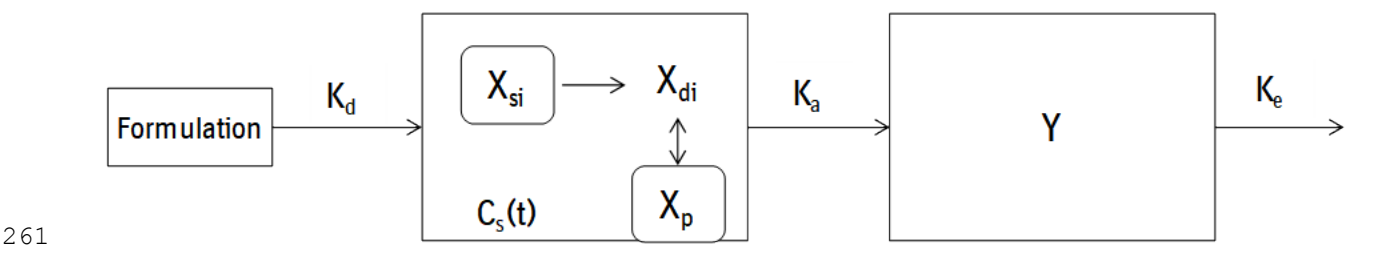


Figure 3 Schematic representation of the dynamic dissolution permeation model

The thickness of diffusion layer, h, is assumed to be constant at 30  $\mu$ m when particle radius is greater or equal to 30  $\mu$ m, while h is equal to the particle radius when the particle radius is less than 30  $\mu$ m. The particle size of the precipitate was assumed to be 1  $\mu$ m. The integration was executed using the deSolve package in R [3].

Dry powder in gavage tubes pre-coated with Mg stearate was administered directly into the stomach, followed by flushing with 1 mL of deionized water. Rats were fasted overnight with food returned after the 4 hours of sampling time. Water was available *ad libitum*. Blood samples

(0.3 mL) were drawn from indwelling jugular cannulas at 0.5, 1, 2, 4, 6, 8, and 24 h after dosing. Blood samples were placed on ice immediately and centrifuged under refrigeration to harvest

plasma. The plasma concentration analysis was performed by LC/MS/MS. A total of 21 rats

were used for each formulation.

Pharmacokinetics study in rats

# Results and Discussion

The solubility values of BI 639667 in various media are listed in Table 1. Precipitation occurs quickly upon pH shifting from acidic to neutral condition for BI 639667. Various techniques have been attempted to increase the oral bioavailability of this compound, including salt formation, amorphous dispersion by spray drying and hot-melt extrusion, nano-suspension, and amorphous silica carrier. No salts with acceptable chemical and physical stability had been identified. Among other formulation techniques, amorphous solid dispersion with HPMC-AS by spray drying showed the best *in vivo* performance and was able to enhance bioavailability by 3 folds relative to crystalline freebase. However, the amorphous dispersions showed high batch-to-batch variance in dissolution. Significant issues during manufacturing were also encountered at a large scale. Moreover, the resulted tablet size was large at dose of 130 mg due to the additional large amount of HPMC-AS from amorphous dispersion. The large tablet size is not desired because it may lead to poor patient compliance. Hence, cocrystal formation was explored as an alternative to achieve sufficient bioavailability enhancement while maintaining good stability and manufacturability.

 Table 1
 Solubility of BI 639667 in various media at room temperature

Medium	Mean solution concentration at 48 hours, μg/ml (n=3)
pH 1.2	187.1
pH 2.0	29.9
pH 3.0	11.3

pH 4.5	8.3
pH 6.8	8.1
pH 8.0	8.0
water	9.4
FaSSIF	19.5
FeSSIF	50.7

# Cocrystal screening

In silico coformer selection was conducted to facilitate cocrystal engineering. Interaction energies between BI 639667 and the selected coformers were calculated as excess enthalpy between API and coformer by the COSMO-RS method. This method had been used to predict solvate and cocrystal formation for 18 APIs [26, 28]. A similar method based on molecular electrostatic potential surfaces is able to predict new solid forms for Sildenafil, where 26 new solid forms had been identified [29]. The interaction energy values were listed in Table 2, where gentisic acid shows the highest cocrystal formation propensity, followed by fumaric acid, tartaric, salicylic, and succinic acid. Although Salicylic acid (SA) bears significant structural similarity to gentisic acid, it ranks only higher than succinic acid. It seems that the number of hydroxyl groups, especially those with conjugated benzene ring or double bonds, could significantly increase the partial charge and resulted in higher interaction energy with API.

**Table 2** Excess enthalpy between BI 639667 and different coformers, calculated using COSMO-RS

Rank	Coformer	excessive
		energy, KCal/mol
1	Gentisic acid	-2.83
2	Fumaric acid	-2.73
3	Tartaric acid	-2.59
4	Salicylic acid	-1.9
5	Succinic acid	-1.48

To validate the prediction from the computational results, experimental screening of BI 639667

Form I was used as the starting material in this study. The DSC thermogram of BI 639667 shows

a melting endotherm of Form I at 193°C, followed by recrystallization to Form V at 197 °C and

melting of Form V at 208 °C. Cocrystal formation during heating would manifest as a sharp

melting at a temperature lower than the melting point of BI 639667 Form I [30]. However, the

thermograms of the systems. Since the DSC experiments were inconclusive, further experiments

1:1 w/w mixtures showed complicated thermal behaviors with multiple diffused endotherms

(Figure 4), which may be explained by eutectic melting phenomenon complicating the

were carried out using a solution/slurry cocrystal screening method.

cocrystal was carried out using DSC to provide a quick readout [30]. The BI 639667 freebase

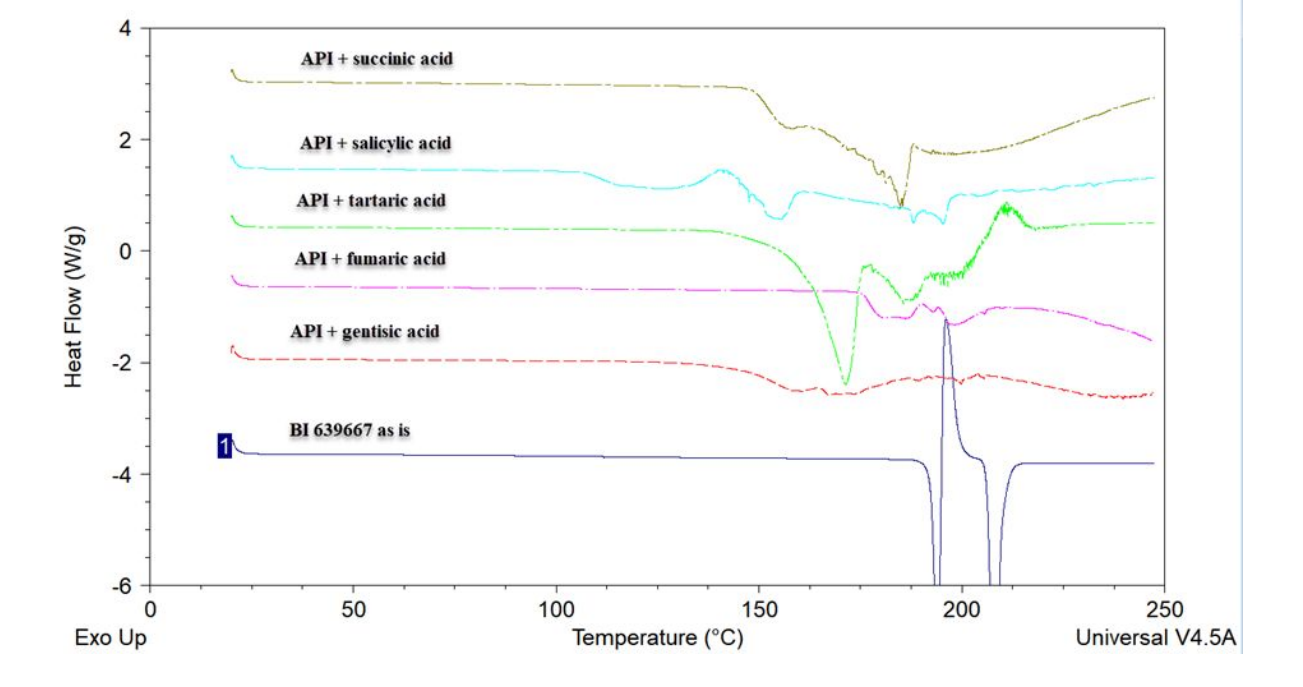


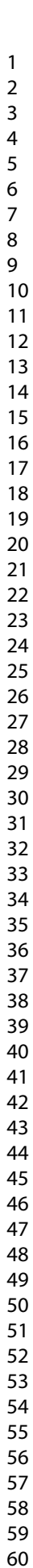
Figure 4 DSC thermograms of binary mixtures of API with selected coformers

Because an adequate solubility is required to facilitate the cocrystal formation in the limited experimental time frame, and different solvent types can vary the polarity, dielectric constant, hydrogen bonding characteristics, and API conformations to enable potential cocrystal formation, solvents play an important role in the crystallization of cocrystal. Therefore, we

determined the solubility of BI 639667 in 16 common organic solvents (Table 3), where four solvents, acetone, acetonitrile, dioxane, and dichloromethane, were selected for solution crystallization experiments because they showed both suitable solubility and diverse solvent characteristics. However, among all 20 combinations (5 coformers and 4 solvents), only a succinic acid cocrystal from ACN and a salicylic acid cocrystal from MeCl<sub>2</sub> were obtained (Figure 5).

**Table 3** Solubility of BI 639667 free base in organic solvents at 20 °C

No	Solvent	Solubility, mg/g
1	Acetone	15.35
2	Acetonitrile	9.36
3	Ethanol	0.97
4	Ethanol:n-Heptane; 1:1, v/v	0.67
5	Ethyl Acetate	2.55
6	Isopropyl Alcohol	0.04
7	Methanol	2.92
8	Methylene Chloride	11.87
9	Nitromethane	0.82
10	Toluene	0.43
11	Water	0
12	ACN:H2O; 1:1, v/v	5.89
13	1,4-Dioxane	20.43
14	THF	80.57
15	MeOH:H2O;1:1, v/v	0.55
16	DMA:H2O;1:1, v/v	2.09



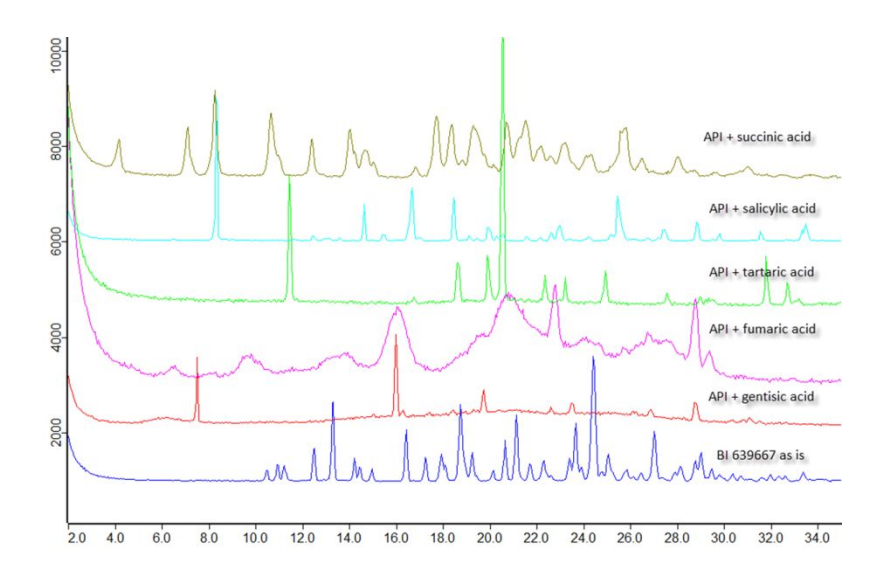


Figure 5 XRPD patterns of BI 639667 and materials obtained from the cocrystallization experiment with selected coformers.

The failure to produce any cocrystal by the DSC method suggests that these cocrystals, if exist, require a longer time to nucleate and grow than the time available during the DSC experimental (20-30 min). The preparation of two least likely forming cocrystals and failure with three more likely forming cocrystals based on the COSMO-RS calculation suggests the binary interaction energy may not be the dominating factor for cocrystal formation. Other factors, such as conformation and packing efficiency, may play important roles.

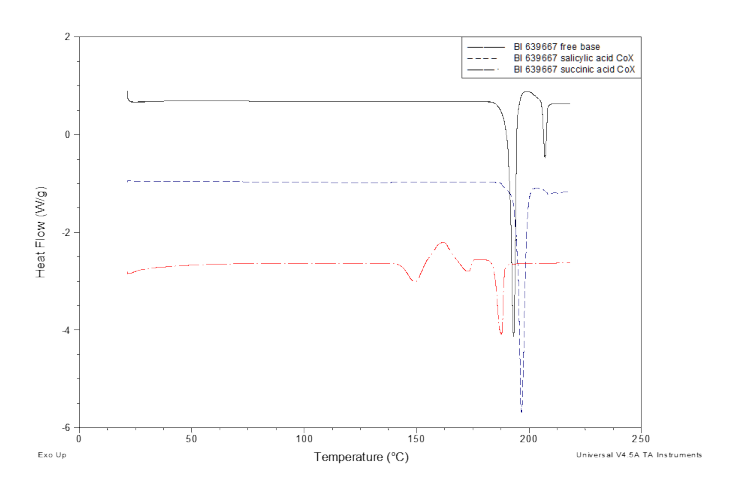
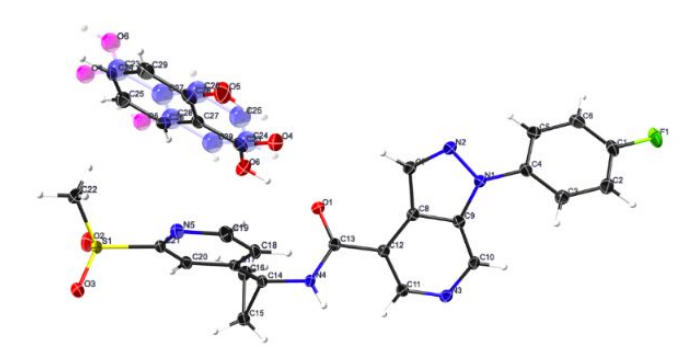


Figure 6 Thermograms of BI 639667 free form and cocrystals with salicylic and succinic acid

The succinic acid cocrystal showed complicated thermal behavior (Figure 6) and a likely polymorph of this cocrystal was observed in a scale up batch. In contrast, the SA cocrystal showed only one polymorph during scale up. The only known SA cocrystal form also shows a simple melting peak during heating, which is higher than that of the free base (Figure 6). Given the less attractive solid-state landscape and complicated thermal behaviors of succinic acid case, only the SA cocrystal was further investigated.

The crystal structure of the SA cocrystal was solved by single crystal X-ray crystallography with a R value of 3.5%. Figure 7 shows the ellipsoid plot of the asymmetric unit, where the SA molecules are disordered over an inversion center. Consequently, the stoichiometry of the cocrystal is 2:1, instead of 1:1, BI 639667:SA [31]. To confirm this unusual stoichiometry, the cocrystal was further analyzed by HPLC. The  $13.6 \pm 0.1\%$  (w/w, n =3) SA content in the cocrystal is close to the theoretical value in a 2:1 BI 639667:SA cocrystal (13.3%, w/w), confirming the correct assignment of the 2:1 stoichiometry. In this structure, BI 639667 molecules form channels running along the *b* axis, which are filled by SA molecules (Figure 8).



**Figure 7** Ellipsoid plot of the asymmetric unit of the BI 639667 - salicylic acid cocrystal. Two disordered SA molecules are shown.

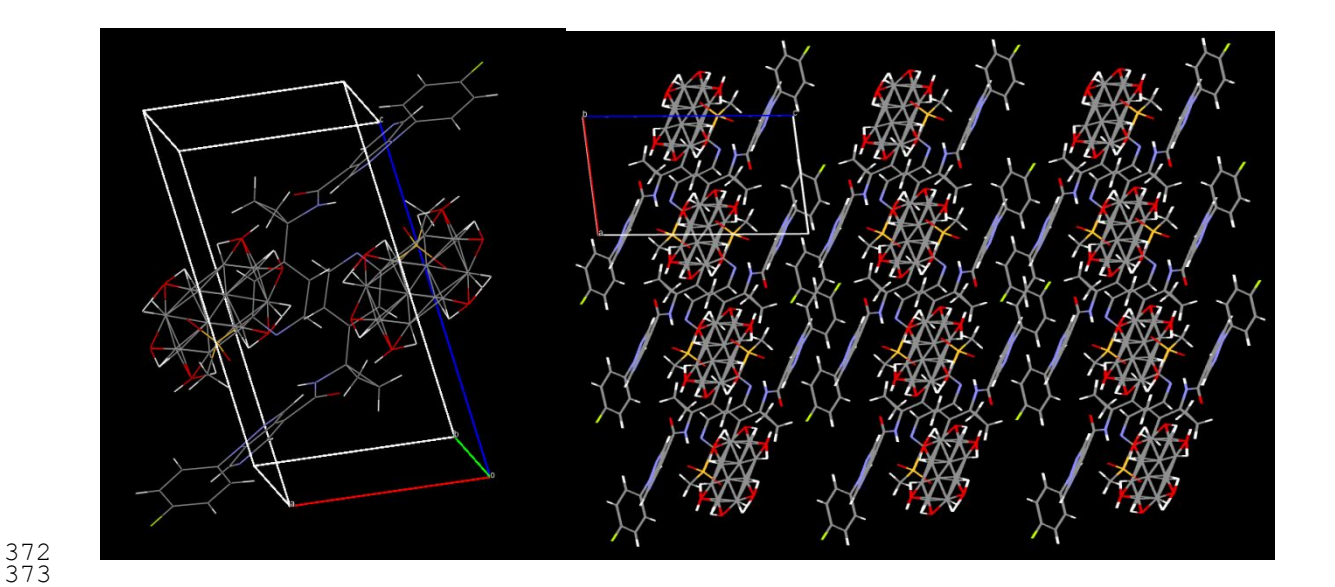


Figure 8 Unit cell (left) and crystal packing (right) of BI 639667 SA cocrystal

The calculated XRPD pattern using the crystal structure determined at 100 K showed slight shift when compared with the experimental pattern obtained at room temperature (Figure 9). This is likely due to thermal expansion from 100K to RT. To test this hypothesis, Rietveld refinement was performed to fit the crystal lattice to the XRPD pattern at room temperature, while fixing the space group and symmetry operations. The Rietveld-refined crystal lattice provided excellent agreement between calculated XRD pattern and the experimental one (Figure 10), confirming the thermal expansion effect.

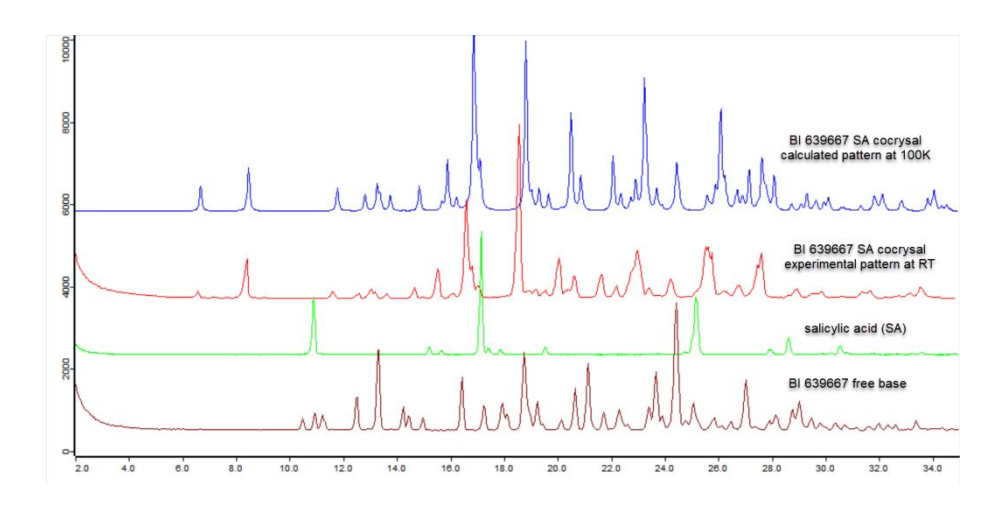
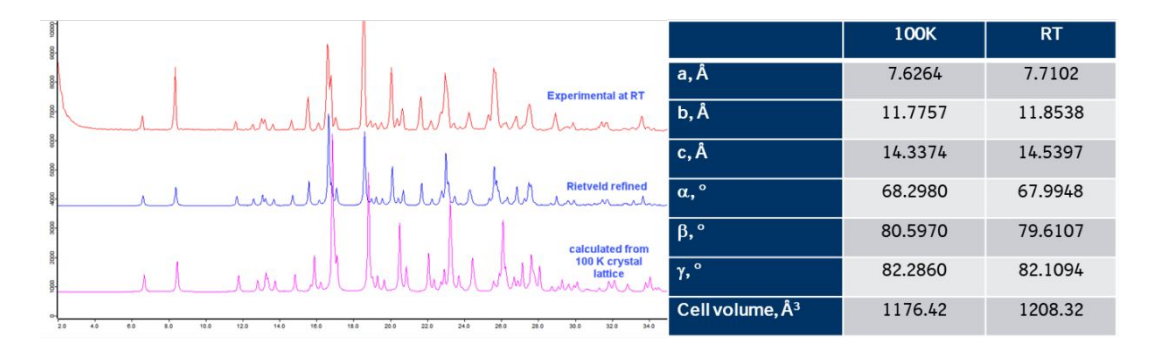


Figure 9 Experimental XRPD patterns of the salicylic acid, BI 639667 free base, and the cocrystal, compared with the calculated XRPD pattern from the crystal structure of the cocrystal



**Figure 10** Rietveld refinement of the cocrystal structure revealed anisotropic expansion of crystal lattice from 100 K to room temperature

# Dissolution and precipitation kinetics

To improve the accuracy of the predicted *in vivo* performance in humans, the ability to maintain supersaturation in solution should be assessed under the physiological conditions [32]. Alternatively, *in vivo* performance could be better predicted by combining biorelevant dissolution testing with biopharmaceutical simulation [33, 34]. In this study, we determined the dissolution profiles of the SA cocrystal using a modified two-step dissolution method. The dissolution profiles were modeled to deconvolute the solubility and precipitation kinetics parameters. The effective permeability of the API was studied in rats. Subsequently, the *in vivo* performance of the SA cocrystal in humans was predicted based on first principles.

The modified two-step dissolution method considers pH, surfactant level, and volume of dissolution media to better match the *in vivo* conditions. In a typical two-step dissolution test [35], simulated gastric fluid (SGF) at pH 1.2 is used as the dissolution media in the first step, followed by adding large volume of concentrated phosphate buffer to obtain a final pH of 6.5. However, the solubility of BI 639667 is highly sensitive to pH within the human gastric pH

range, usually 1 - 3 [36], with the solubility at pH 1.2 being 6 times of that at pH 2. Thus, using SGF would lead to a high degree of supersaturation and fast precipitation upon pH switch, which may not be the case in a real human GI tract. Therefore, we modified the method by using a pH 2 HCl solution instead of SGF in the first dissolution step. Additionally, we used a small volume of saturated phosphate solution to adjust the pH to 6.0 in the second step. This modification is to minimize the volume change during pH switch because the volume of dissolution media may significantly impact the bioavailability prediction, as reported for BMS-480188 [37]. In fact, the volume of GI fluid would gradually decrease after gastric emptying in the small intestine. The average intestinal liquid is only 100 mL for humans, even after drinking 240 mL water [38, 39], due to the absorption of water and nutrition in the small intestine. The third and last modification was to add a small amount of bile salt and lecithin based on the composition of Fasted state simulated intestinal fluid (FaSSIF) [40]. In summary, the routine two-step dissolution conditions.

The ability to maintain supersaturation upon a change in medium of crystalline freebase, amorphous spray-dried dispersion (SDD), and SA cocrystal was compared based on their dissolution profiles using the modified two-step dissolution method (Figure 11). The SDD showed the fastest dissolution in pH 2. The solution concentration increased initially in the second step due to the solubilization by bile salt, which was followed by fast precipitation within 5 min. The salicylic acid (SA) cocrystal showed a reduced concentration, compared with that of crystalline freebase. In the second step, the SA cocrystal showed a small increase in concentration and slow precipitation during the following 2 hours. Dissolution profiles were modelled using the modified Johnson equation to capture the key parameters of the dissolution and precipitation kinetics (Table 5). The modeling result indicated that the SDD was able to increase the API concentration in both simulated gastric and intestinal fluids. However, the precipitation rate of SDD was comparable to that of crystalline freebase in the second dissolution step, with a half-life of 5 and 2 min, respectively. Among the three solid forms, the SA cocrystal showed the lowest API concentration in the simulated gastric fluid but was able to maintain the longest period of supersaturation.

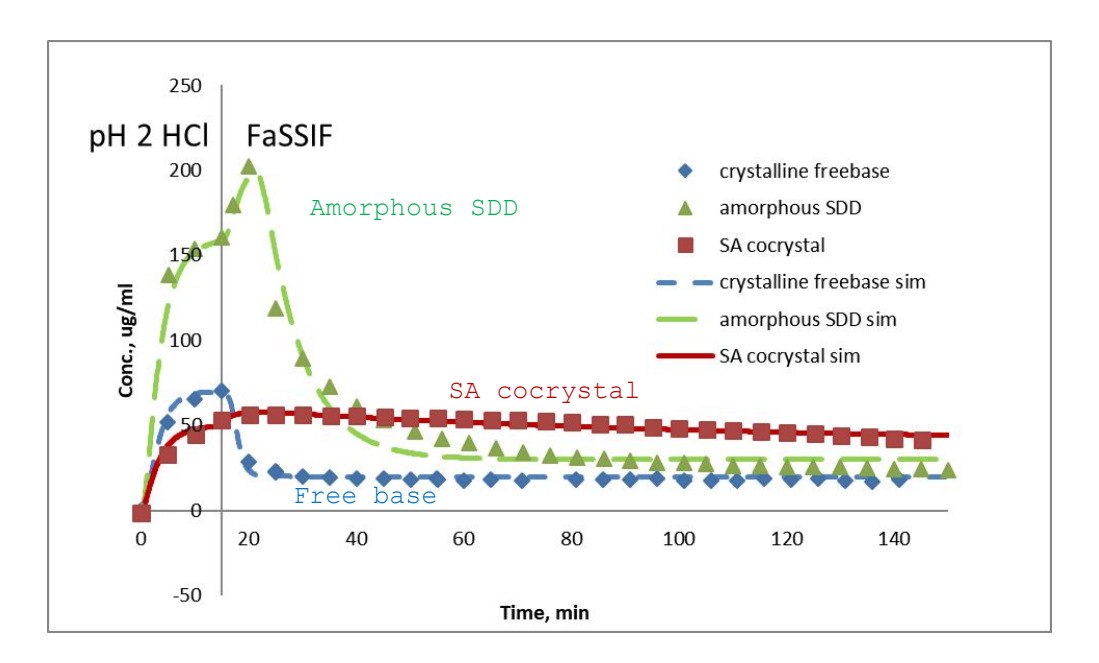


Figure 11 Experimental (points) and simulated (lines) two-step dissolution profiles of 140 mg of BI 639667 free base, compared with equivalent free base amounts for cocrystals with salicylic acid (SA) and amorphous dispersion, using a modified two-step dissolution method (first step: 300 mL of pH 2 HCl solution; second step: 320 mL of FaSSIF solution at pH 6.0 - 6.2, pH switch at 15 min)

**Table 4** Dissolution model parameters for particle size, solubility, and precipitation kinetics using Johnson equations

Input	Amorphous dispersion	Free form	SA
Apparent particle size	30	50	50
Conc. in stomach, mg/mL	0.17	0.07	0.05
Initial conc. in intestine,	0.35	0.02	0.06
mg/mL			
Final conc. in intestine,	0.03	0.02	0.04
mg/mL			

Half precipitation time by	5	2	70
first-order, min			

# 

465
466

Half precipitation time by	5	2	70
first-order, min			

# Rat study and prediction in humans

The *in vivo* performance of the crystalline freebase, amorphous SDD, and SA cocrystal were studied in rats, and the results were shown in Table 7. When the dose is 30 mg/kg, the SA cocrystal shows a slightly lower AUC and approximately half of the  $C_{\text{max}}$  when compared to the amorphous dispersion. The *in vivo* performance correlates well with prolonged supersaturation and a reduced kinetic solubility of the SA cocrystal in FaSSIF. The reduced Cmax correlates well with the reduced cocrystal solubility in both steps of the dissolution test. The prolonged supersaturation explains the comparable AUC despite the C<sub>max</sub> is only about 50% of that of the amorphous dispersion. This lower  $C_{\text{max}}$  is advantageous since it may potentially reduce the toxicity of the drug. The solution formulation contains large amount of VE-TPGS, and shows no precipitation when diluted with equal volume of SGF or SIF. Therefore, it is reasonable to assume a 100% absorption for the solution formulation considering the high permeability of BI 639667 across Caco2 cell membrane. The relative bioavailability for SA cocrystal and amorphous dispersion could be considered equivalent to the fraction absorbed.

Table 5 *In vivo* exposure in rats following oral administration of powders containing different BI 639667 solid forms at 30 mg/kg, compared with the simulated values in rats and humans

Group	Delivery system	C <sub>max</sub> (nM)	AUC <sub>0-24h</sub>	Relative BA	Simulated Fa in	Simulated Fa in
			(nM*h)	(%)	rats at 30 mg/kg	humans at 140 mg
						dose
1	Solution	13,900	94,100	100	100	100
2	free base	3,462	21,479	23	21	4-8
3	Amorphous dispersion	15,200	65,200	69	46	8-16
4	SA Cocrystal	7,420	54,200	58	41	8-16

We further performed biopharmaceutical simulations to predict the bioavailability in humans. The bioavailability in humans may also be estimated as the mean value of those in animal models. However, a large survey showed no correlation between fraction absorbed (Fa) in animal models and in humans [41]. In contrast, the effective permeability in humans has been shown to correlate well with that in rat [42]. Other preclinical permeability models, such as caco-2 cell and PAMPA membranes, may suffer from lack of representative influx or efflux transporters [43, 44]. The overall simulation strategy is to first estimate the effective absorption constant from the rat study result. The oral absorption in humans is then simulated based on the solubility/precipitation kinetics (Table 5) and using the regional absorption rates and liquid volumes based on literature reports (Table 6) [45, 46]. The gastrointestinal transit times are based on the report from Dressman [36]. The regional absorption rate in the small intestine is arbitrarily set at 10 fold higher than that in the colon, which includes the effect of reduced surface area in colon. Due to the uncertainty of the precise estimation on human effective permeability, the absorption rate constant in humans is set to be 1/3 to 2/3 of that in rats based on a report from Lennernaes [47]. The liquid volume values for rats and humans are based on the report from McConnell [48] and Schiller [38], respectively.

The simulation results suggest that the SA cocrystal may have similar bioavailability to that of the amorphous dispersion in humans (Table 5). The simulation under-predicted the bioavailability of amorphous SDD and SA cocrystal in rats (Table 5), which may be explained by high bile salt levels in rat intestines compared with that in humans due to the lack of gallbladders in rats [49, 50]. The bile salt may enhance the solubility of the amorphous dispersion more than that of the cocrystal.

**Table 6** Major physiological parameters for PK Profile Simulation in rats and humans

Inputs	Rat	Human
Regional absorption rate		
constant, 1/min		
0 - 30 min	0	0
30-270 min	0.05	0.02-0.04

270-830 min	0.01	0.004-0.008
Liquid volumes, ml		
stomach	10	300
Small intestine	3	100
colon	1	30

# Effect of supersaturation ratio on precipitation kinetics

The mechanism of bioavailability enhancement for high energy solid forms, including salts and cocrystals, has been qualitatively explained as spring-and-parachute effect [18], where parachute refers to the slow precipitation so that a meaningful bioavailability increase can be achieved. A recent study showed poor correlation between the initial cocrystal solubility and the *in vivo* performance of cocrystals, while the supersaturation duration during *in vitro* dissolution could better predict the *in vivo* performance [25].

One mechanism for SA cocrystal's supersaturation maintenance could be that the cocrystal's reduced solubility leads to lower supersaturation degree and therefore a slower precipitation. To test this hypothesis, we studied the effect of supersaturation on the precipitation kinetics in FaSSIF using the solvent shift method. The highest supersaturation ratio is 12 (200  $\mu$ g/mL), corresponding to the maximum concentration of amorphous dispersion observed during dissolution in FaSSIF. The lowest supersaturation ratio is 3 (50  $\mu$ g/mL), corresponding to the maximum concentration of SA cocrystal in FaSSIF. The supersaturation level did have some impact on the precipitation induction time (Figure 12). An induction time of 10 min was observed at 50  $\mu$ g/mL, while the induction time was 2 min for 200  $\mu$ g/mL and 5 min for 100  $\mu$ g/mL. In comparison, the SA cocrystal was able to maintain a 3-fold supersaturation for up to two hours, which is drastically longer than the precipitation time of the free base at a similar API concentrations (10 min). Therefore, the long induction time, or supersaturation duration, of SA cocrystal precipitation cannot be explained by the reduction in the solubility of cocrystal or supersaturation level alone.

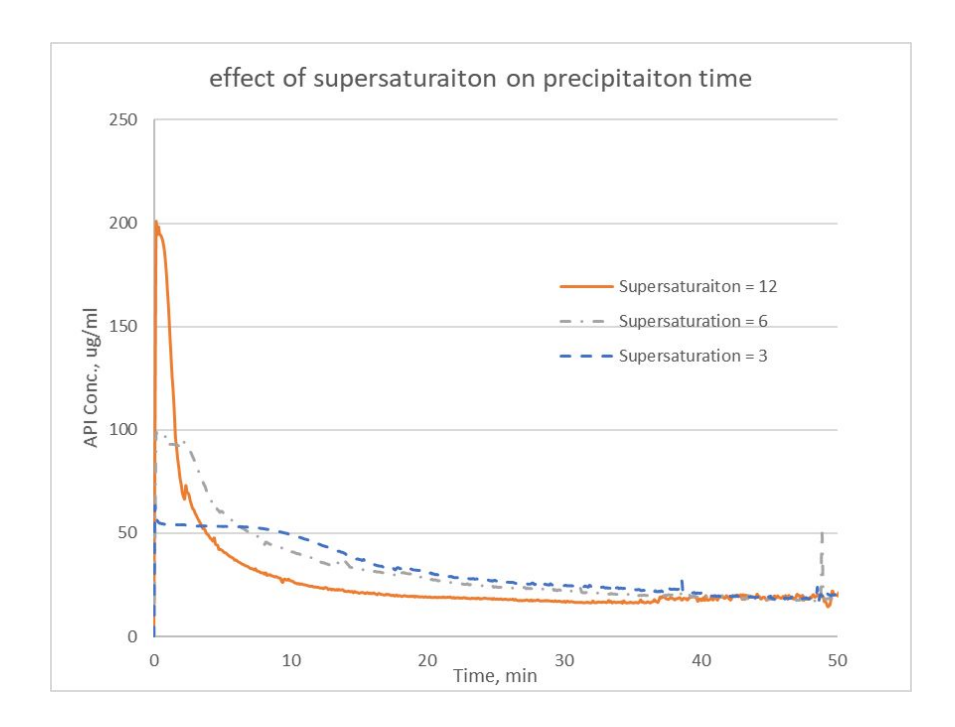
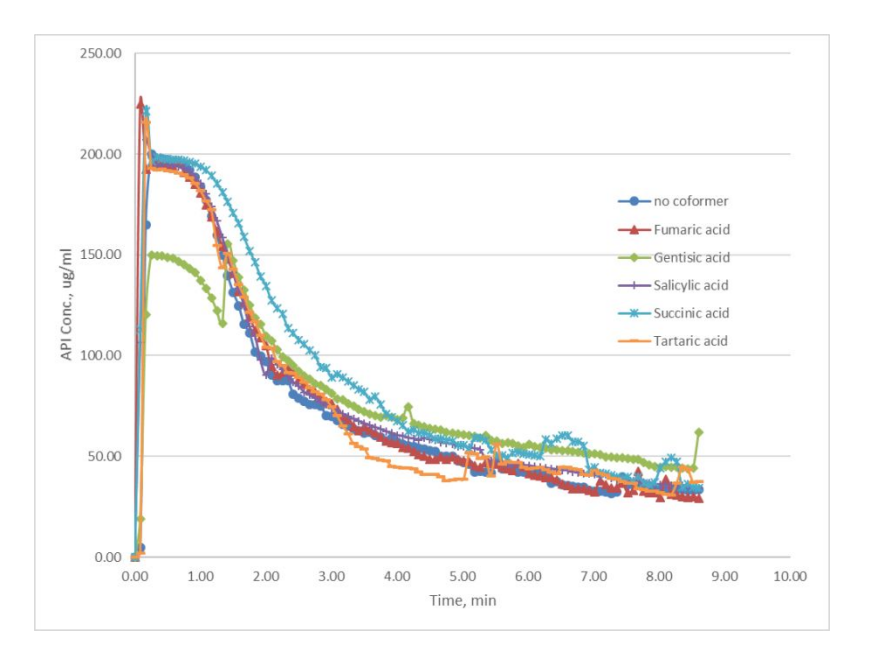


Figure 12 The impact of starting supersaturation level on the induction time for precipitation monitored by UV fiber optic probes (n=2)

It is also possible that SA could prolong supersaturation of BI 639667 in solution through certain specific solute-solute interactions. If so, we may be able to use solvent shift method, similar to the ones used for screening polymer precipitation inhibitors [51], to exclude "bad" coformers that would not form bioavailability enhancing cocrystals. The effect of the five coformers on the precipitation kinetics of BI 639667 was studied in FaSSIF at an initial API concentration of 200 µg/mL (supersaturated ratio of 12 relative to the free base) with the coformer at 3 times that of the API on a molar basis. Rapid precipitation was observed in all cases, with a half precipitation time around 3 min (Figure 13). Thus, it can be concluded that the presence of coformer showed little impact on the precipitation kinetics of the API in FaSSIF in all cases. This lack of precipitation inhibition for salicylic acid seems contradictory to the long supersaturation observed for the SA cocrystal. It is possible that nuclei of BI 639667 may have already formed during the initial mixing of DMSO and water, especially at the interface. Coformers, being nonsurface active small molecules, could not adhere to the surfaces of nuclei and inhibit crystal growth as polymers could do [52]. This result shows that coformers screen using the solvent shift may not effective to determine its potential to form bioavailability enhancing cocrystals.



**Figure 13** Concentration of BI 639667 with time showing the effect of coformer on the precipitation kinetics of BI 639667 in fasted state simulated intestinal fluid

# Molecular Dynamics Simulation

Although the SA cocrystal's ability to maintain supersaturation is likely due to its ability to inhibit nucleation of the API, it is challenging to experimentally study the nucleation process of BI 639667 due to its fast precipitation process (with a half-life of precipitation of 2 min), and lack of instruments to study the microscopic process. Therefore, we performed virtual experiments using molecular dynamics simulations to examine the nucleation down to the nanosecond and atomic level. Molecular dynamic simulation could be a powerful tool to understand the crystallization, especially the nucleation process [53, 54]. We used an explicit solvent model to account for various types of intermolecular interactions, including H-bonding,  $\pi$ - $\pi$  interaction, and van der Waal forces. We constructed a simulation box with API, water, and coformer and allowed water molecules to compete with the coformer for hydrogen bonding with the API.

The impact of coformers on API nucleation was first studied by visualizing the self-association of API molecules in aqueous media. Self-association of solute molecules to form molecular clusters has been widely considered a precursor for nucleation, and the structure of the molecular clusters could determine the kinetics and outcome of crystallization [55-58]. The simulation result shows that BI 639667 readily formed large molecular clusters in the simulation box filled with water molecules (Figure 12), which is consistent with its rapid precipitation kinetics observed during dissolution and solvent shift experiments. This rapid cluster formation could be driven by strong  $\pi$ - $\pi$  intermolecular interactions between the aromatic groups in the API molecules, such as pyrazolopyrimidines, benzene, and pyridine. The coformer molecules (red in Figure 14) was able to penetrate the API cluster (blue in Figure 14), with different degrees of penetration for different coformers. For example, compared with succinic acid, salicylic acid showed more penetration into the API molecular cluster due to its benzene ring and less hydrophilic groups.

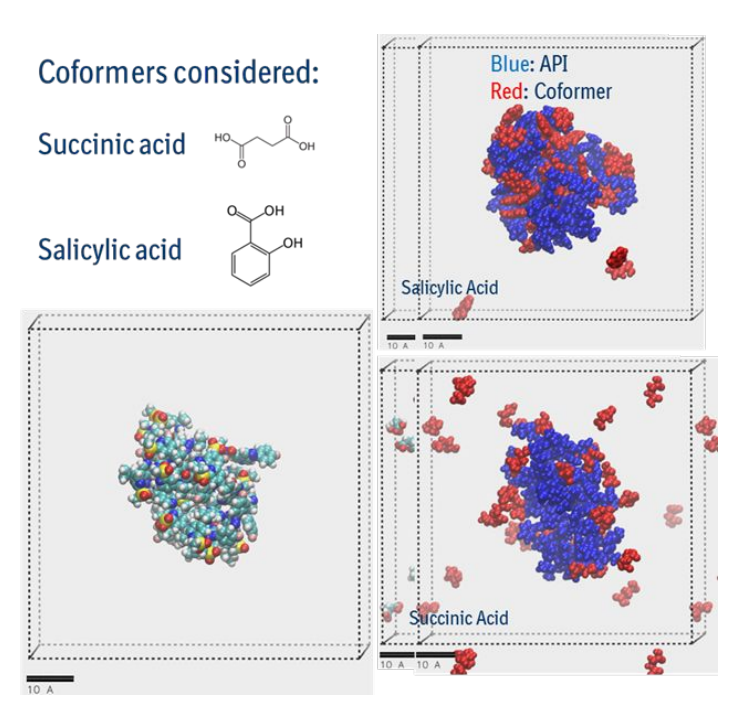


**Figure 14** Formation of API molecular clusters in aqueous solution using molecular dynamics simulations and ability of coformer molecules to penetrate the API molecular clusters. BI 639667 (blue), conformer (red)

The strength of API coformer interaction in the presence of water can be further quantified as the radial distribution function (RDF, g(r)), which is defined as the possibility of finding the coformer molecule at different distances from the API molecules. Stronger interactions between API and coformer molecules, in spite of the competition from water, would result in smaller RDF values. Based on the RDF curves in an aqueous solution, the rank-order for the strength of interaction between coformer and API follows the descending order of SA > GE > FU > TA > SC (Figure 15). Compared with the rank-order by interaction energy in a vacuum (GE > FU > TA > SA > SC), the RDF method predicts the strongest interactions between API and SA in water, which correlates well with the strong ability of SA to maintain supersaturation during dissolution and higher bioavailability.

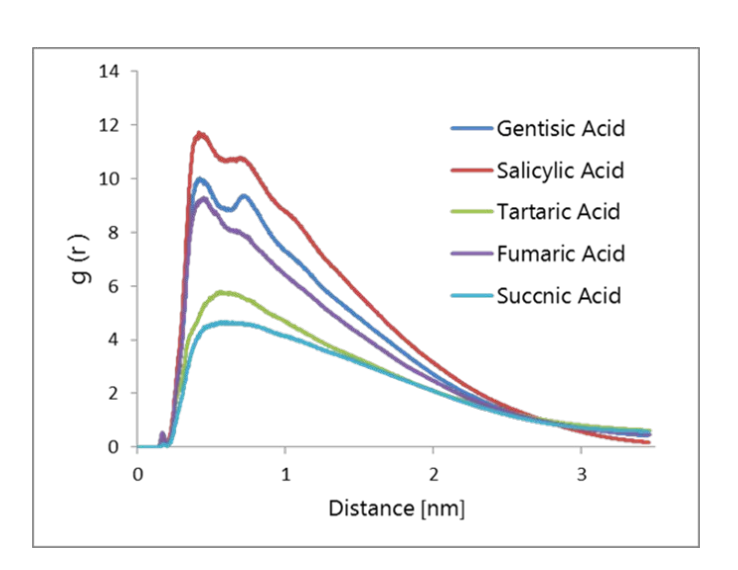


**Figure 15** Radial distribution function (RDF, g(r)) between BI 639667 and different coformers in aqueous solution

Thus, the cocrystal' ability to maintain supersaturation in aqueous media may be better predicted by the interaction energy between coformer and API in water than that in a vacuum. The interaction energy in a vacuum is calculated as the sum of intermolecular forces, including electrostatic, hydrogen bonds, and van der Waals forces. However, water is a polar molecule and can form strong hydrogen bonds, which would compete with the coformer molecules for the

interaction sites on the API molecules. Water could impact hydrogen bonding and polar-polar interactions more than it could impact  $\pi$ - $\pi$  interaction and hydrophobic forces. Hydrogen bonds and polar-polar interactions are strong forces that may contribute the most to the overall binary interaction energy in a vacuum. Therefore, the actual interaction between coformer and API in aqueous media may differ drastically from the calculated value in a vacuum. Salicylic acid ranks the highest in terms of the strength of the interaction with API in aqueous media, while only second to last in a vacuum. This may be explained by its benzene ring and fewer hydrophilic groups, such as hydroxyl and carboxylic acid. To engineer cocrystals for bioavailability enhancement, it may be important to select coformers that could compete with water for interactions with API, which may better inhibit nucleation and maintain supersaturation during dissolution. The radius distribution function (g(r)), calculated by MD simulation of ternary system containing API, coformer, and water, could be an alternative indicator of a coformer's ability to maintain supersaturation and achieve enhanced bioavailability.

# Conclusion

Cocrystal engineering for bioavailability enhancement is presently still a trial and error exercise. The SA cocrystal of BI 639667 was able to maintain long supersaturation during *in vitro* dissolution and bioavailability in rats. The ability of the SA cocrystal to maintain supersaturation was not predicted by the current *in silico* interaction energy theory, which ignored the competing effect of water on hydrogen bonding interactions between API and coformers.

Our results suggest that the ability of a coformer to compete against water for interactions with API may be an important factor to understand the ability to maintain supersaturation and to enhance bioavailability. To this end, the radius distribution function (RDF), which describes the average distance or closeness between coformer and API in an aqueous solution, is a useful tool. This novel indicator may help us select coformers that could better maintain supersaturation during dissolution to achieve successful development of bioavailability enhancing cocrystals for poorly soluble compounds.

# Acknowledgement

We thank Drs. Chen-Ming Lee and Guanfa Gan for coordinating the rat studies. G.V. is partially funded by a grant from the National Science Foundation (grant number IIP- 1919037) Y.G. is partially supported by a Doctoral Dissertation Fellowship (2020 – 2021) and David J.W. Grant & Marilyn J. Grant Fellowship in Physical Pharmacy (2020 – 2021) of University of Minnesota.

Supporting information is available, including the crystal structure CIF file and structure refinement details for the BI 639667 salicylic acid cocrystal

# References:

- 1. Aitipamula, S., R. Banerjee, A.K. Bansal, K. Biradha, M.L. Cheney, A.R. Choudhury, G.R. Desiraju, A.G. Dikundwar, R. Dubey, N. Duggirala, P.P. Ghogale, S. Ghosh, P.K. Goswami, N.R. Goud, R.R.K.R. Jetti, P. Karpinski, P. Kaushik, D. Kumar, V. Kumar, B. Moulton, A. Mukherjee, G. Mukherjee, A.S. Myerson, V. Puri, A. Ramanan, T. Rajamannar, C.M. Reddy, N. Rodriguez-Hornedo, R.D. Rogers, T.N.G. Row, P. Sanphui, N. Shan, G. Shete, A. Singh, C.C. Sun, J.A. Swift, R. Thaimattam, T.S. Thakur, R. Kumar Thaper, S.P. Thomas, S. Tothadi, V.R. Vangala, N. Variankaval, P. Vishweshwar, D.R. Weyna, and M.J. Zaworotko, Polymorphs, Salts, and Cocrystals: What's in a Name? *Cryst. Growth Des.* **2012**, 12, 2147-2152
- 2. Wohler, F., Untersuchungen über des chinons. *Ann Chem Pharm* **1844**, 145.
- 3. Etter, M.C., Encoding and decoding hydrogen-bond patterns of organic compounds. *Acc. Chem. Res.* **1990**, 23, 120-6.
- 4. Desiraju, G.R., Supramolecular synthons in crystal engineering a new organic synthesis. *Angew. Chem., Int. Ed. Engl.* **1995**, 34, 2311-27.
- 5. Sun, C.C., Cocrystallization for successful drug delivery. *Expert Opinion on Drug Delivery* **2013**, 10, 201-213.
- 6. Wong, S.N., Y.C.S. Chen, B. Xuan, C.C. Sun, and S.F. Chow, Cocrystal Engineering of Pharmaceutical Solids: Therapeutic Potentials and Challenges. *CrystEngComm* **2021**.
- 7. Wang, L., S. Liu, J.-m. Chen, Y.-x. Wang, and C.C. Sun, Novel Salt-Cocrystals of Berberine Hydrochloride with Aliphatic Dicarboxylic Acids: Odd–Even Alternation in Physicochemical Properties. *Molecular Pharmaceutics* **2021**, 18, 1758-1767.
- 8. Liang, Z., H. Chen, C. Wang, and C.C. Sun, Discovery, Characterization, and Pharmaceutical Applications of Two Loratadine–Oxalic Acid Cocrystals. *Crystals* **2020**, 10, 996.
- 9. Li, J., X. Hao, C. Wang, H. Liu, L. Liu, X. He, and C.C. Sun, Improving the Solubility, Dissolution, and Bioavailability of Metronidazole via Cocrystallization with Ethyl Gallate. *Pharmaceutics* **2021**, 13, 546.
- 10. Chen, H., Y. Guo, C. Wang, J. Dun, and C.C. Sun, Spherical Cocrystallization—An Enabling Technology for the Development of High Dose Direct Compression Tablets of Poorly Soluble Drugs. *Crystal Growth & Design* **2019**, 19, 2503-2510.

- 11. Zhao, X., Q. Li, C. Wang, S. Hu, X. He, and C.C. Sun, Simultaneous taste-masking and oral bioavailability enhancement of Ligustrazine by forming sweet salts. *International Journal of Pharmaceutics* **2020**, 577, 119089
- 12. Liu, F., L.-Y. Wang, M.-C. Yu, Y.-T. Li, Z.-Y. Wu, and C.-W. Yan, A new cocrystal of isoniazid-quercetin with hepatoprotective effect: The design, structure, and in vitro/in vivo performance evaluation. *European Journal of Pharmaceutical Sciences* **2020**, 144, 105216.
- 13. FDA, Regulatory Classification of Pharmaceutical Co-Crystals Guidance for Industry. 2018, <a href="https://www.fda.gov/media/81824/download">https://www.fda.gov/media/81824/download</a>.
- 14. Sun, C.C. and H. Hou, Improving Mechanical Properties of Caffeine and Methyl Gallate Crystals by Cocrystallization. *Cryst. Growth Des.* **2008**, 8, 1575-1579.
- 15. Holaň, J., F. Štěpánek, P. Billot, and L. Ridvan, The construction, prediction and measurement of co-crystal ternary phase diagrams as a tool for solvent selection. *European Journal of Pharmaceutical Sciences* **2014**, 63, 124-131.
- 16. Hunter, C.A. and R. Prohens, Solid form and solubility. *CrystEngComm* **2017**, 19, 23-26.
- 17. Kuminek, G., F. Cao, A. Bahia de Oliveira da Rocha, S. Goncalves Cardoso, and N. Rodriguez-Hornedo, Cocrystals to facilitate delivery of poorly soluble compounds beyond-rule-of-5. *Adv. Drug Delivery Rev.* **2016**, 101, 143-166.
- 18. Babu, N.J. and A. Nangia, Solubility Advantage of Amorphous Drugs and Pharmaceutical Cocrystals. *Cryst. Growth Des.* **2011**, 11, 2662-2679.
- 19. Kale, D.P., S.S. Zode, and A.K. Bansal, Challenges in Translational Development of Pharmaceutical Cocrystals. *J. Pharm. Sci.* **2016**, Ahead of Print.
- Bak, A., A. Gore, E. Yanez, M. Stanton, S. Tufekcic, R. Syed, A. Akrami, M. Rose, S. Surapaneni, T. Bostick, A. King, S. Neervannan, D. Ostovic, and A. Koparkar, The co-crystal approach to improve the exposure of a water-insoluble compound: AMG 517 sorbic acid co-crystal characterization and pharmacokinetics. *J. Pharm. Sci.* 2008, 97, 3942-3956.
- 21. Shan, N., M.L. Perry, D.R. Weyna, and M.J. Zaworotko, Impact of pharmaceutical cocrystals: the effects on drug pharmacokinetics. *Expert Opin. Drug Metab. Toxicol.* **2014**, 10, 1255-1271.
- Almeida e Sousa, L., S.M. Reutzel-Edens, G.A. Stephenson, and L.S. Taylor, Supersaturation Potential of Salt, Co-Crystal, and Amorphous Forms of a Model Weak Base. Crystal Growth & Design 2016, 16, 737-
- 23. Yamashita, H. and C.C. Sun, Harvesting Potential Dissolution Advantages of Soluble Cocrystals by Depressing Precipitation Using the Common Coformer Effect. *Cryst. Growth Des.* **2016**, 16, 6719-6721.
- Wang, C., Q. Tong, X. Hou, S. Hu, J. Fang, and C.C. Sun, Enhancing Bioavailability of Dihydromyricetin through Inhibiting Precipitation of Soluble Cocrystals by a Crystallization Inhibitor. *Cryst. Growth Des.* **2016**, 16, 5030-5039.
- 25. Yoshimura, M., M. Miyake, T. Kawato, M. Bando, M. Toda, Y. Kato, T. Fukami, and T. Ozeki, Impact of the Dissolution Profile of the Cilostazol Cocrystal with Supersaturation on the Oral Bioavailability. *Cryst. Growth Des.* **2017**, 17, 550-557.
- 26. Abramov, Y.A., C. Loschen, and A. Klamt, Rational Coformer or Solvent Selection for Pharmaceutical Cocrystallization or Desolvation. *Journal of Pharmaceutical Sciences* **2012**, 101, 3687-3697.
- 27. Hübschle, C.B., G.M. Sheldrick, and B. Dittrich, ShelXle: a Qt graphical user interface for SHELXL. *Journal of applied crystallography* **2011**, 44, 1281-1284.
- 28. Loschen, C. and A. Klamt, Solubility prediction, solvate and cocrystal screening as tools for rational crystal engineering. *Journal of Pharmacy and Pharmacology* **2015**, 67, 803-811.
- 29. Barbas, R., M. Font-Bardia, A. Paradkar, C.A. Hunter, and R. Prohens, Combined Virtual/Experimental Multicomponent Solid Forms Screening of Sildenafil: New Salts, Cocrystals, and Hybrid Salt–Cocrystals. *Crystal Growth & Design* **2018**, 18, 7618-7627.
- 30. Lu, E., N. Rodríguez-Hornedo, and R. Suryanarayanan, A rapid thermal method for cocrystal screening. *CrystEngComm* **2008**, 10, 665-668.
- 31. Kratzert, D. and I. Krossing, Recent improvements in DSR. *Journal of Applied Crystallography* **2018**, 51, 928-934.
- 32. Dressman, J.B. and C. Reppas, In vitro-in vivo correlations for lipophilic, poorly water-soluble drugs. *Eur. J. Pharm. Sci.* **2000**, 11, S73-S80.
- 33. Lennernaes, H., A. Lindahl, A. Van Peer, C. Ollier, T. Flanagan, R. Lionberger, A. Nordmark, S. Yamashita, L. Yu, G.L. Amidon, V. Fischer, E. Sjoegren, P. Zane, M. McAllister, and B. Abrahamsson, In

- Vivo Predictive Dissolution (IPD) and Biopharmaceutical Modeling and Simulation: Future Use of Modern Approaches and Methodologies in a Regulatory Context. *Mol. Pharmaceutics* **2017**, 14, 1307-1314.
- 34. Klumpp, L. and J. Dressman, Physiologically based pharmacokinetic model outputs depend on dissolution data and their input: Case examples glibenclamide and dipyridamole. *Eur. J. Pharm. Sci.* **2020**, 151, 105380.
- Mann, J., J. Dressman, K. Rosenblatt, L. Ashworth, U. Muenster, K. Frank, P. Hutchins, J. Williams, L. Klumpp, and K. Wielockx, Validation of dissolution testing with biorelevant media: an OrBiTo study.
   Molecular pharmaceutics 2017, 14, 4192-4201.
- 36. Dressman, J.B., Comparison of canine and human gastrointestinal physiology. *Pharm. Res.* **1986**, 3, 123-31.
- 37. Gu, C.-H., R.B. Gandhi, L.K. Tay, S. Zhou, and K. Raghavan, Importance of using physiologically relevant volume of dissolution medium to correlate the oral exposure of formulations of BMS-480188 mesylate. *International Journal of Pharmaceutics* **2004**, 269, 195-202.
- 38. Schiller, C., C.P. Frohlich, T. Giessmann, W. Siegmund, H. Monnikes, N. Hosten, and W. Weitschies, Intestinal fluid volumes and transit of dosage forms as assessed by magnetic resonance imaging. *Aliment Pharmacol Ther* **2005**, 22, 971-9.
- 39. Mudie, D.M., K. Murray, C.L. Hoad, S.E. Pritchard, M.C. Garnett, G.L. Amidon, P.A. Gowland, R.C. Spiller, G.E. Amidon, and L. Marciani, Quantification of Gastrointestinal Liquid Volumes and Distribution Following a 240 mL Dose of Water in the Fasted State. *Molecular Pharmaceutics* **2014**, 11, 3039-3047.
- 40. Galia, E., E. Nicolaides, D. Hörter, R. Löbenberg, C. Reppas, and J.B. Dressman, Evaluation of Various Dissolution Media for Predicting In Vivo Performance of Class I and II Drugs. *Pharmaceutical Research* **1998**, 15, 698-705.
- 41. Cao, X., S.T. Gibbs, L. Fang, H.A. Miller, C.P. Landowski, H.-C. Shin, H. Lennernas, Y. Zhong, G.L. Amidon, L.X. Yu, and D. Sun, Why is it Challenging to Predict Intestinal Drug Absorption and Oral Bioavailability in Human Using Rat Model. *Pharm. Res.* **2006**, 23, 1675-1686.
- 42. Chiou, W.L. and A. Barve, Linear correlation of the fraction of oral dose absorbed of 64 drugs between humans and rats. *Pharm. Res.* **1998**, 15, 1792-1795.
- 43. Lennernaes, H., Human jejunal effective permeability and its correlation with preclinical drug absorption models. *J. Pharm. Pharmacol.* **1997**, 49, 627-638.
- 44. Ren, S. and E.J. Lien, Caco-2 cell permeability vs human gastrointestinal absorption: QSPR analysis. *Prog Drug Res* **2000**, 54, 1-23.
- Walsh, P.L., J. Stellabott, R. Nofsinger, W. Xu, D. Levorse, K. Galipeau, and F. Kesisoglou, Comparing Dog and Human Intestinal Fluids: Implications on Solubility and Biopharmaceutical Risk Assessment. *AAPS PharmSciTech* **2017**, 18, 1408-1416.
- 46. Willmann, S., W. Schmitt, J. Keldenich, J. Lippert, and J.B. Dressman, A Physiological Model for the Estimation of the Fraction Dose Absorbed in Humans. *J. Med. Chem.* **2004**, 47, 4022-4031.
- 47. Lennernaes, H., Human Intestinal Permeability. J. Pharm. Sci. 1998, 87, 403-410.
- 48. McConnell, E.L., A.W. Basit, and S. Murdan, Measurements of rat and mouse gastrointestinal pH, fluid and lymphoid tissue, and implications for in-vivo experiments. *Journal of Pharmacy and Pharmacology* **2008**, 60, 63-70.
- 49. Yusuke, T., H. Toshihiro, W. Ryoichi, and N. Shunji, Regional Differences in the Components of Luminal Water from Rat Gastrointestinal Tract and Comparison with Other Species. *Journal of Pharmacy and Pharmaceutical Sciences* **2012**, 15.
- 50. Christfort, J.F., S. Strindberg, J. Plum, J. Hall-Andersen, C. Janfelt, L.H. Nielsen, and A. Mullertz, Developing a predictive in vitro dissolution model based on gastrointestinal fluid characterisation in rats. *Eur. J. Pharm. Biopharm.* **2019**, 142, 307-314.
- 51. Price, D.J., F. Ditzinger, N.J. Koehl, S. Jankovic, G. Tsakiridou, A. Nair, R. Holm, M. Kuentz, J.B. Dressman, and C. Saal, Approaches to increase mechanistic understanding and aid in the selection of precipitation inhibitors for supersaturating formulations a PEARRL review. *The Journal of pharmacy and pharmacology* **2019**, 71, 483-509.
- 52. Gao, Y. and K.W. Olsen, Drug-Polymer Interactions at Water-Crystal Interfaces and Implications for Crystallization Inhibition: Molecular Dynamics Simulations of Amphiphilic Block Copolymer Interactions with Tolazamide Crystals. *J. Pharm. Sci.* **2015**, 104, 2132-2141.
- Gaines, E., K. Maisuria, and D. Di Tommaso, The role of solvent in the self-assembly of m-aminobenzoic acid: a density functional theory and molecular dynamics study. *CrystEngComm* **2016**, 18, 2937-2948.

- 54. Hamad, S., C. Moon, C.R.A. Catlow, A.T. Hulme, and S.L. Price, Kinetic Insights into the Role of the Solvent in the Polymorphism of 5-Fluorouracil from Molecular Dynamics Simulations. *J. Phys. Chem. B* **2006**, 110, 3323-3329.
- 55. Davey, R.J., K.R. Back, and R.A. Sullivan, Crystal nucleation from solutions transition states, rate determining steps and complexity. *Faraday Discuss.* **2015**, 179, 9-26.
- Du, W., A.J. Cruz-Cabeza, S. Woutersen, R.J. Davey, and Q. Yin, Can the study of self-assembly in solution lead to a good model for the nucleation pathway? The case of tolfenamic acid. *Chem. Sci.* **2015**, 6, 3515-3524.
- 57. Tang, W., H. Mo, M. Zhang, S. Parkin, J. Gong, J. Wang, and T. Li, Persistent self-association of solute molecules in solution. *J. Phys. Chem. B* **2017**, 121, 10118-10124.
- 58. Chen, D., Q. Sun, W. Huang, and B.-S. Yang, Diverse Solvent Selection for Polymorph Landscape Investigation Based on Specific API–Solvent Interactions. *Crystal Growth & Design* **2020**, 20, 2251-2265.

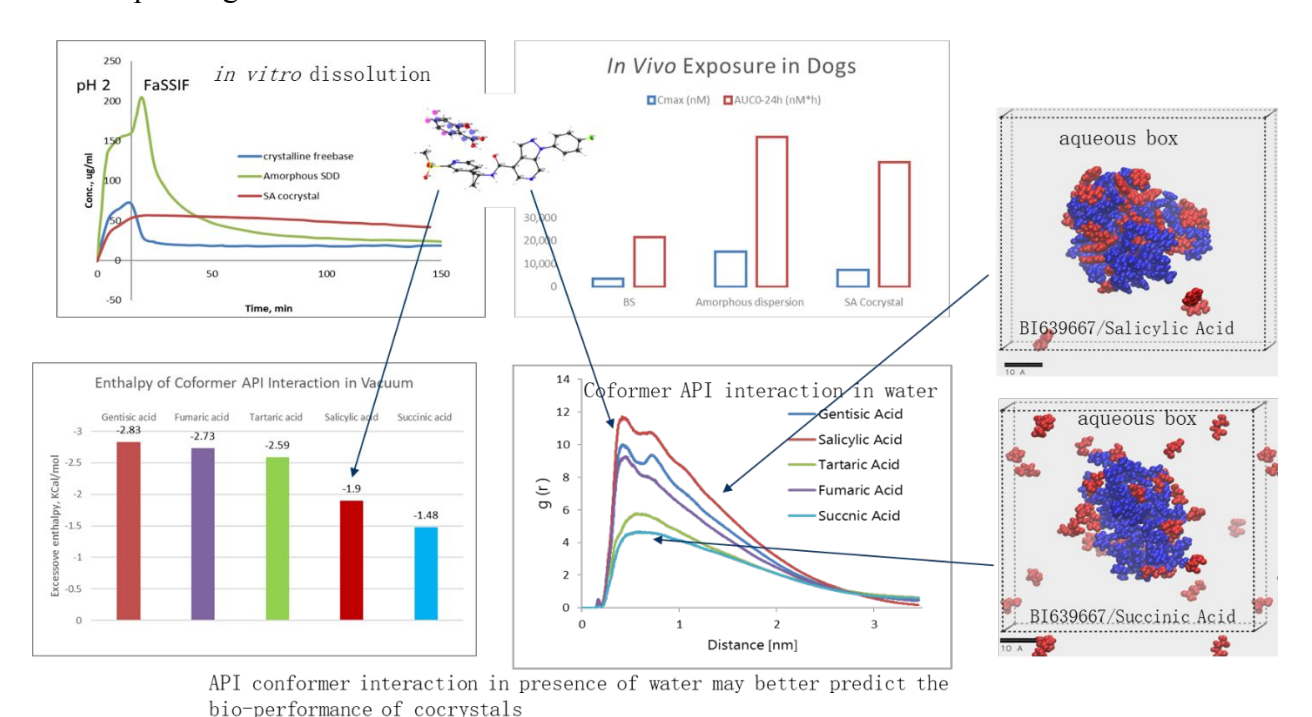
# For Table of Contents Use Only

Bioavailability Enhancing Cocrystals: screening, in vivo predictive dissolution, and supersaturation maintenance

Dabing Chen<sup>1,3\*</sup>, Wenjun Huang<sup>1</sup>, Qinfang Zhang<sup>1</sup>, Zenghui Zhang<sup>1</sup>, Yiwang Guo<sup>2</sup>, Gerrit Vreeman<sup>2</sup>, Changquan Calvin Sun<sup>2\*</sup>, Michael Hawley<sup>1</sup>, Bing-Shiou Yang<sup>1</sup>, Xiaorong He<sup>1</sup>

College of Pharmacy, University of Minnesota, Minneapolis, MN 55455, United States

# \* corresponding authors



**'eywords**: Bioavailability Cocrystal Supersaturation *In vivo* predicative disse

**Keywords**: Bioavailability, Cocrystal, Supersaturation, *In vivo* predicative dissolution, Biopharmaceutical simulation, Molecular dynamics

<sup>&</sup>lt;sup>1</sup> Boehringer Ingelheim Pharmaceuticals Inc., 900 Ridgebury Road, Ridgefield, CT 06877, USA

<sup>&</sup>lt;sup>2</sup> Pharmaceutical Materials Science and Engineering Laboratory, Department of Pharmaceutics,

<sup>&</sup>lt;sup>3</sup> Currently Formulation R&D, Arvinas, New Haven, CT 06510, USA